Original Research

Magnetic Resonance Imaging in Renal Transplantation

Mohammed A. Neimatallah, MB, ChB,* Qian Dong, MD, Stefan O. Schoenberg, MD, Kyung J. Cho, MD, and Martin R. Prince, MD, PhD

End stage renal disease is common and can result from a variety of diseases. The expense and morbidity of dialysis has made renal transplantation the preferred treatment when it is available. In the United States, 11,000 renal transplants are performed annually. Because of the limited supply of donor organs, every effort is made to salvage the transplanted kidney that has began to fail. Imaging modalities that are currently used to evaluate transplanted kidneys are ultrasound (US), computed tomography (CT), scintigraphy, intravenous urography (IVU), contrast angiography, and magnetic resonance imaging (MRI). MRI offers multiple advantages. MRI provides cross sectional and vascular information without the risks of ionizing radiation, iodinated contrast, or arterial catheterization. This article describes the role of MR imaging in renal transplantation, technical aspects of image acquisition, and MR findings of post-transplantation complications. J. Magn. Reson. Imaging 1999;10:357–368. © **1999 Wiley-Liss, Inc.**

MR IMAGING OF POTENTIAL DONORS

Since there is increased complexity of surgery and potential risk to the donor kidney during surgery when there are anatomic variations, pretransplantation assessment of the renal vascular anatomy of the potential renal donor is an important step (2–7). The incidence of variant arterial anatomy of the kidney is 40%, including early renal artery division or branches, multiple renal arteries (aberrant and accessory renal arteries), and multiple renal veins. Multiple renal arteries occur in 30% of the population (8). Angiography has been the primary imaging modality for the evaluation of renal vascular anatomy. In addition to finding accessory renal arteries and renal arterial pathology, angiography obtains information about the length of the main renal artery before division. A length of at least 2 cm is preferred for surgical anastomosis (9,11). Although conventional angiography is the gold standard it is an invasive procedure. Because of the risks of allergic reaction, nephrotoxicity from the use of iodinated contrast, hematoma, intimal wall injury, and thrombosis, non-invasive imaging methods are preferred.

In the last few years, 3D-Gd MRA has advanced to the point that most of renal vascular anatomy can be accurately demonstrated (Fig. 1). Recent studies have reported excellent sensitivity and accuracy in the depiction of accessory renal arteries, using conventional angiography as the standard of reference (2,3,10–13). MRI also has the advantage of assessing the donor renal parenchyma for masses or cysts. CT angiography is also promising for evaluation of renal donors, although it does not eliminate the risk of iodinated contrast nor ionizing radiation.

Using MR hydrography (SSFSE = single shot fast spin echo, HASTE = half Fourier single shot turbo spin echo) or 3D contrast-enhanced MRU, it is possible to assess the collecting system as well as the ureters. Low et al. reported a comprehensive MR examination for the potential renal transplant donor, including 3D enhanced-MRA, MR urography, and MR nephrography (3).

SURGICAL ASPECTS OF RENAL TRANSPLANTATION

Knowledge of the surgical anatomy of the renal allograft and its post surgical complications is fundamental for imaging of the renal allograft. There are several surgical approaches to renal transplantation: the standard pelvic approach (intra or extraperitoneal), pediatric en-bloc approach, lower abdominal approach (if there have been more than two prior transplants), and orthotopic approach (Fig. 2a–c).

The donor left kidney is preferred when there are no anomalies because the longer left renal vein facilitates the venous anastomosis (14). Simultaneous kidney-pancreas transplantation is a preferred option for treating end stage renal disease in patients with type I diabetes mellitus (Fig. 3) (1).

MR IMAGING TECHNIQUES

MRI has a variety of sequences that can obtain information about anatomy, function, flow, and lesion characterization. The pelvic location of the renal allograft minimizes motion artifact related to respiration particu-

Department of Radiology, University of Michigan Medical Center, Ann Arbor, Michigan and Cornell University Medical Center, New York, NY (MRP).

Contract grant sponsor: The Whitaker Foundation; Contract grant sponsor: Deutsche Forschungsgemeinschaft (DFG).

*Address reprint requests to: M.A.N. University of Michigan Medical Center, Department of Radiology-MRI Division, 1500 East Medical Center Drive, Ann Arbor, MI 48109-0030.

Received June 14, 1999; Accepted June 14, 1999.

Figure 1. Coronal MIP reconstruction of breath-hold 3D Gd-MRA. Bilateral accessory renal arteries arising from the abdominal aorta.

larly if the torso coil is secured tight around the pelvis to restrict abdominal wall motion. Administration of antispasmodic drugs such as glucagon or Hyosen-N-butylbromide (buscopan) can be helpful in improving the image quality by reducing the bowel motion. Previous abdominal and pelvic radiographs should be reviewed for the presence of surgical clips in the transplant region since this may produce confusing metallic artifact (15). Prior to the examination, the patient is rested in a quite room for relaxation. In claustrophobic patients, mild sedation may be required. In adult patients, 5–10 mg of diazepam or 1–2 mg Xanay is given orally 20–30 minutes before the examination. An 18 or 20 gauge angiocatheter is inserted in the antecubital

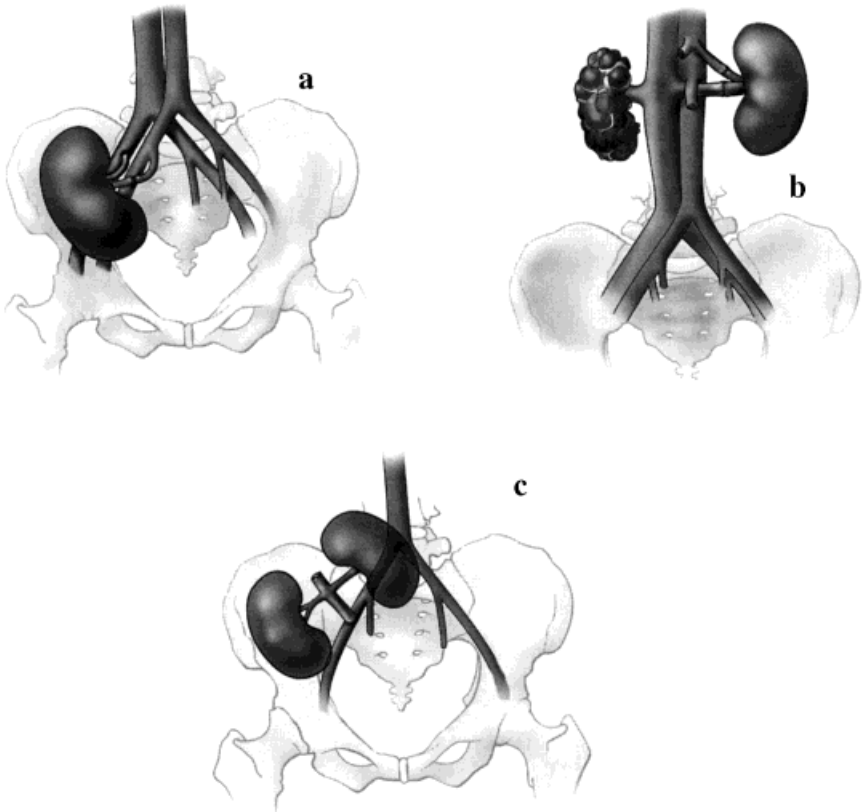

Figure 2. Illustrations showing different surgical approaches to renal transplantation. Basic pelvic approach (**a**), Orthotopic (**b**), and pediatric En-block approach (**c**).

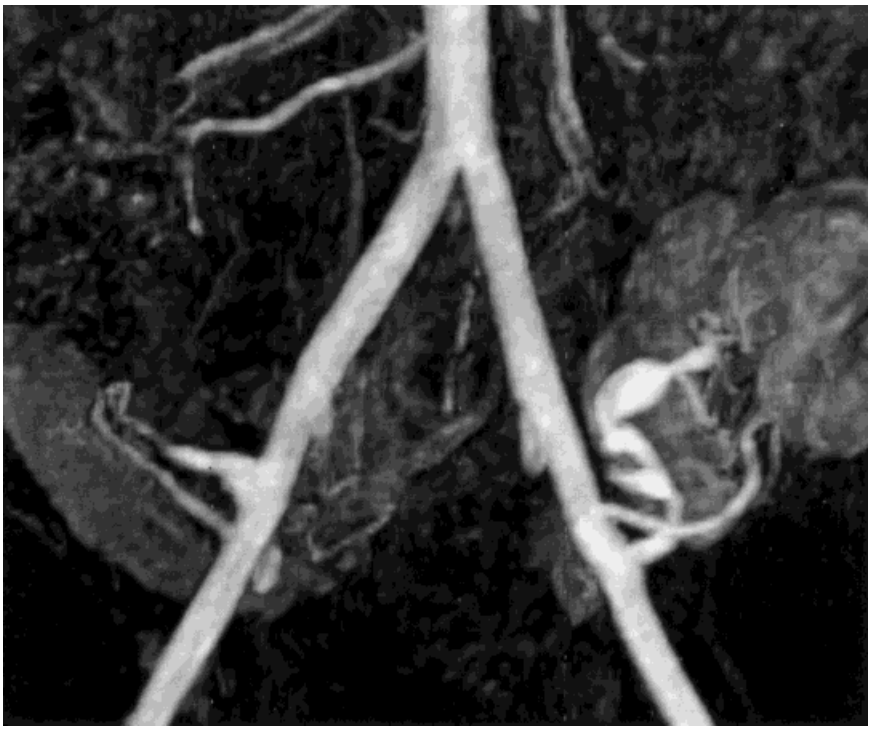

Figure 3. Coronal MIP reformat from 3D Gd-MRA in a patient who had simultaneous kidney-pancreas transplantation demonstrating main and accessory arteries supplying the transplant kidney (open arrows) and two arteries supplying the pancreatic transplants (arrowhead). Notice the multiple aneurysms involving the transplant main renal artery related to prior pancreatitis of the transplant (small arrow).

vein and connected to the tubing set flushed with saline ready for contrast injection.

Imaging begins with a large field-of-view coronal locator sequence such as Single Shot Fast Spin Echo (SSFSE) or T1 weighted spin echo sequence (Fig. 4). The SSFSE sequence is preferred because it is fast and does not require breath holding. In addition it allows for the evaluation of pelvicalyceal system for hydronephrosis and perinephric fluid collections. The imaging parameters are summarized in Table 1.

Figure 4. Locator SSFSE in coronal plane demonstrating the renal allograft and a large peritransplant fluid collection compressing the renal allograft (*). A lymphocele was confirmed with US guided aspiration.

The second sequence is sagital T1 weighted sequence is used to assess the position, size, and shape and the corticomedullary differentiation (CMD) of the renal allograft. The CMD is even better evaluated with T1 WI with fat saturation or immediate post gadolinium images.

The third sequence is axial T2 fast spin echo sequence with fat saturation. It is graphically prescribed from the sagital locator, starting at the iliac crest and extending down to the level of the sympysis pubis (Fig. 5a). This sequence is useful to assess perinephric fluid collections. If the fluid collection is high in signal on both T1 and T2 weighted images (WI) hematoma or abscess is the possible diagnosis. Peripheral enhancement in T1 weighted images post gadolinium will favor abscess. If the collection is dark in signal on T1 WI but high on T2 WI, the possibility of diagnosis lymphocele, seroma, or urinoma should be considered for the differential diagnosis.

Coronal three-dimensional gadolinium-enhanced magnetic resonance angiography (3D Gd-MRA) should encompass the lower abdominal aorta and extend down to the femoral head. A large field-of-view typically 36 cm (32–40) should be used. Commonly 38 (28–44) partitions each about 2.4 mm thick (2–3.4 mm) are required to cover the aorta, iliac arteries, and renal allograft (Fig. 5b). Zero filling is useful to increase interpolated resolution in the slice direction by two fold (Table 1). The shortest TR should be used to shorten the scan time to

Table 1
Summary of Imaging Parameters*

	Coronal SSFSE locator	Sagital T1 spin echo	Axial T2 FSE with fat sat	Coronal 3D Gd-MRA	Axial 3D PC-MRA	Optional axial 2D TOF
FOV (cm)	40 (32–48)	34	32 (26–44)	34 (30–44)	28 (26–40)	32 (26–44)
TR/TE (ms)	∝/180	400/10	3000/102	6.1/1.3	20/7.4	30/7
Flip angle	—	—		45	35	45
NEX	1	2	4	0.5 (0.5–1)	1	2
Matrix (freq. × pha.)	256 × 256	256 × 256	256 × 256	256/(128/256)	256 × 192	256 × 128
Slice (mm)	8	7	8	2.6 (2–4)	2.5	3
Spacing	0	Interleave	2	0	0	0

*FSE = fast spin echo, TOF = Time-of-Flight, freq = frequency encoding, pha = phase encoding, FOV = field of view, 3D = three dimensional, 2D = two dimensional.

acquire the 3D data in a single breath-hold (Fig. 6a,c). It should be 30–40 seconds for patients with a normal respiratory capacity and less than 30 seconds in patients who are short of breath. Hyperventilating the patient and/or giving oxygen is useful to lengthen the breath-hold capacity. Partial Fourier imaging (0.5 NEX) is another useful way to shorten the scan time without sacrificing resolution. However, partial Fourier imaging increases the risk of having minor ringing artifacts. Shortening the scan time can also be achieved by increasing the slice thickness. Shortening the scan time by using wider bandwidth is less useful since this incurs a severe SNR penalty. Typically 32 kHz is the widest bandwidth we use but with dedicated coils, wider bandwidth might be acceptable.

Three-dimensional phase-contrast MRA (3D PC-MRA) is then performed in the axial plane prescribed from the 3D Gd-MRA images (Fig. 7a). Phase-contrast MRA takes advantage of the previously injected gadolinium contrast to increase the signal-noise ratio (Fig. 6b). This sequence is useful in assessing the severity of renal vascular stenosis (Table 2). The high sensitivity of this sequence has been reported by other investigators; Silverman et al. reported a sensitivity of phase-contrast cine MRA of 100% (16–18). The combination of phased-contrast MRA and 3D Gd-MRA can provide a high level of confidence in detecting allograft vascular disease.

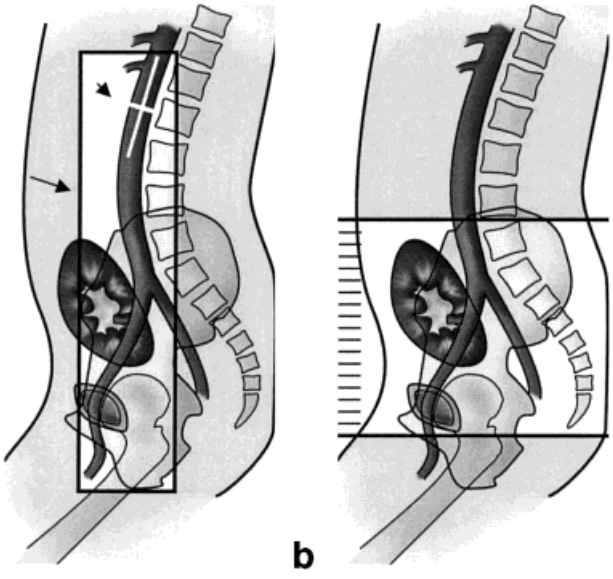

Figure 5. Illustration of sagital locator demonstrating positioning Volume (**a**), for Coronal 3D Gd-MRA with tracker position in the aorta (arrowhead), and (**b**) the Scanning Range for Axial T2.

Additional sequences such as two-dimensional Time-of-Flight (2D TOF) in the axial plane or occasionally in coronal plane may be graphically prescribed from the coronal 3D Gd-MRA to cover the entire allograft to better evaluate venous anatomy and to look for enhancing abnormalities (Fig. 7b). Another capability of MR is to evaluate the allograft blood flow. This is done using breath-hold cine phase-contrast perpendicular to the renal artery to measure the transplant renal artery blood flow. Changes in the time-resolved velocity indicate hemodynamic abnormality (19).

MR renography can be used for the evaluation of the renal function by acquiring rapid repeated breath-hold coronal images of the same position of the kidney every 4–6 seconds using unspoiled gradient echo following the administration of 0.1 mmol/kg of body weight gadopentate dimeglumine (GD-DTPA). Plotting signal-intensity vs. time in the cortex and medulla allows quantitative assessment of the allograft function (20,21). Ros et al. and Sharma et al. reported good agreement between the signal intensity curves obtained with MR renography using gadopentate dimeglumine and the curves obtained with ^{99m}Tc-DTPA renography. They also found that the global GFR values calculated from the total body clearance of gadopentate dimeglumine correlated well with the GFR values calculated from total clearance of ^{99m}Tc-DTPA indicating that MR renography is a feasible technique (22,23).

MR urography provides information about the urinary tract similar to conventional intravenous urography; it can be performed using the rapid acquisition with relaxation enhancement (RARE), half Fourier RARE, contrast-enhanced three-dimensional gradient echo sequence during the excretion phase, or 2D saturation inversion projection images (24,25). A T1 WI with fat saturation in axial plane after gadolinium contrast injection is performed if a mass has been suspected in the peritransplant region or within the renal allograft on ultrasound. MRI can characterize the mass and help in differentiating lymphoproliferative disorder, lymphoma, infection, hematoma, and infarct.

Figure 6. Normal anastomosis of the transplant artery with the right external iliac artery. (**a**) Coronal oblique MIP reconstruction of breath-hold 3D Gd-MRA, (**b**) 3D phase-contrast MRA and (**c**) venous phase of bolus showing normal transplant vein.

MR IMAGING CHARACTERISTICS OF NORMAL RENAL TRANSPLANTATION

The perinephric fat that surrounds the renal allograft should be clear. The renal allograft is uniform in contour with well-defined corticomedullary differentiation on T1 WI. The renal allograft has intermediate to high signal on T2 WI and the CMD is not well seen. When gadolinium contrast is injected, the renal cortex enhances first within 10–20 seconds after bolus injection, followed by medullary enhancement at 20–30 seconds. The CMD should be assessed during early cortical enhancement because later there is homogenous enhancement of the renal parenchyma. Gadolinium chelate appears in the collecting system 3–5 minutes after the start of injection. Concentrated excreted gadolinium chelate in the collecting system may appear as signal void or blooming due to T2* effect. On the other hand, diluted gadolinium chelate produces bright signal.

POSTTRANSPLANTATION COMPLICATIONS

Posttransplantation complications can be grouped as surgical or medical. Immediate complication attributable to surgical difficulties include renal artery thrombosis or stenosis, renal vein thrombosis, urinary leak, or lymphocele. Medical complications include rejection, cyclosporine toxicity, acute tubular necrosis (ATN), infection, and transplantation-related malignancies such

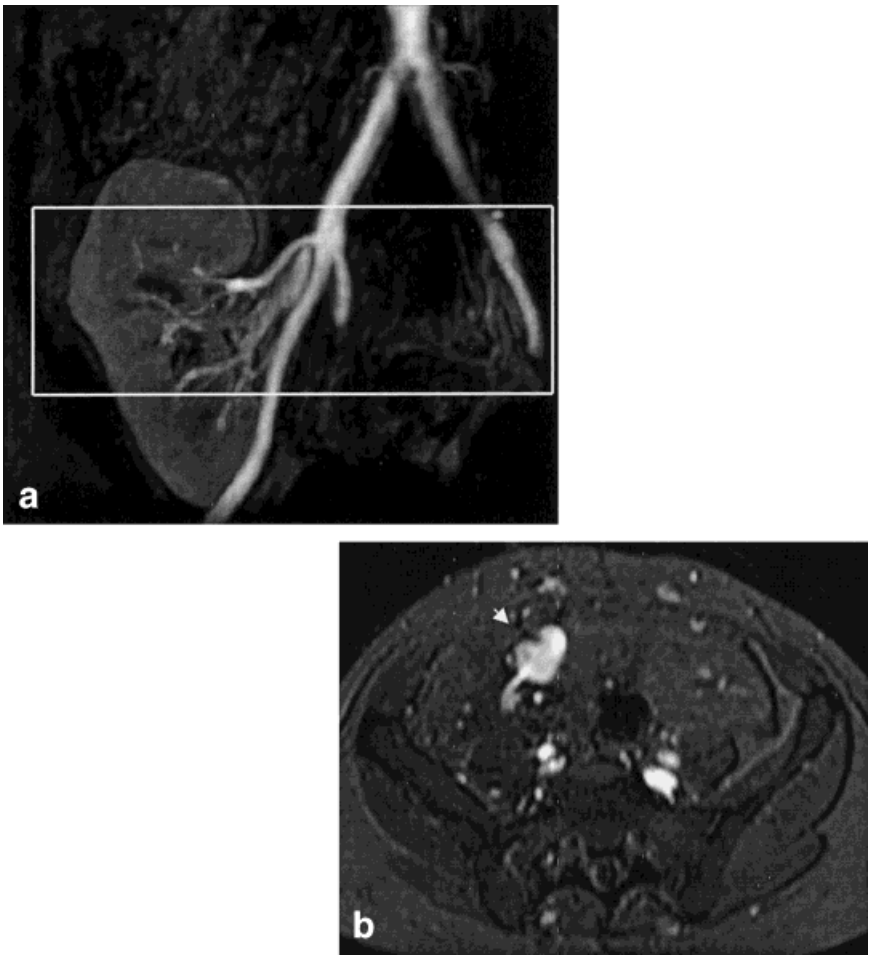

Figure 7. (**a**) Coronal MIP from 3D Gd-MRA demonstrating positioning Volume for axial 3D PC-MRA. (**b**) Axial 2D TOF of the pelvis obtained after 3D Gd-MRA showing iliac vein aneurysm (arrowhead) as complication of prior pancreatitis in patient with simultaneous kidney-pancreas transplantation.

as posttransplantation lymphoproliferative disorder (PTLD) and lymphoma.

Renal Artery Stenosis

Allograft renal artery stenosis occurs in 2 to 10% of cases. It may be caused by intimal hyperplasia at the site of anastomosis, intraoperative trauma of the transplant artery, or atherosclerosis of the donor vessel. It may occur as early as 2 days or as late as several years. Clinically it presents with refractory hypertension and/or deterioration of renal function. A bruit may be audible on auscultation. Early diagnosis and successful treatment of the arterial stenosis prevents premature loss of the allograft. Percutaneous transluminal angioplasty (PTA) is safe and effective and considered the best approach in managing renal artery stenosis, particularly if the stenosis is not at the anastomosis site (26). A surgical approach is preferred for the anastomotic stenosis but there is a risk of sacrificing the allograft due to adhesions from prior surgery. Conventional angiography or contrast enhanced CT have been infrequently used for diagnosing renal artery stenosis because many patients with renal artery stenosis are at higher risk for iodinated contrast induced renal failure.

Three-dimensional contrast enhanced-MRA (3D Gd-MRA) is an appropriate substitute for conventional angiography since it is non-invasive, free of nephrotoxicity, has high spatial resolution, and accurately depicts the transplant vascular anatomy (4,11–13,27–29). The combination of 3D phase-contrast MRA and 3D Gd-MRA increases the accuracy and sensitivity to detect and grade the severity of the stenosis (Fig. 8a). Our scheme used to evaluate renal artery stenosis is summarized in Table 2. In cine phase-contrast flow measurements the hemodynamic significance of the stenosis is indicated by a loss of the early systolic peak in the velocity profile.

Table 2
Scheme in Evaluating Transplant Renal Artery for RAS

3D Gd-MRA	3D PC-MRA	Suggested diagnosis
Normal	Normal	Normal
Normal	Dephasing	Artifact/Inaccurate VENC
Mild stenosis	No dephasing	Not significant stenosis
Moderate/severe stenosis	No dephasing	Stenosis of uncertain significance
Moderate/severe stenosis	Dephasing	Significant stenosis

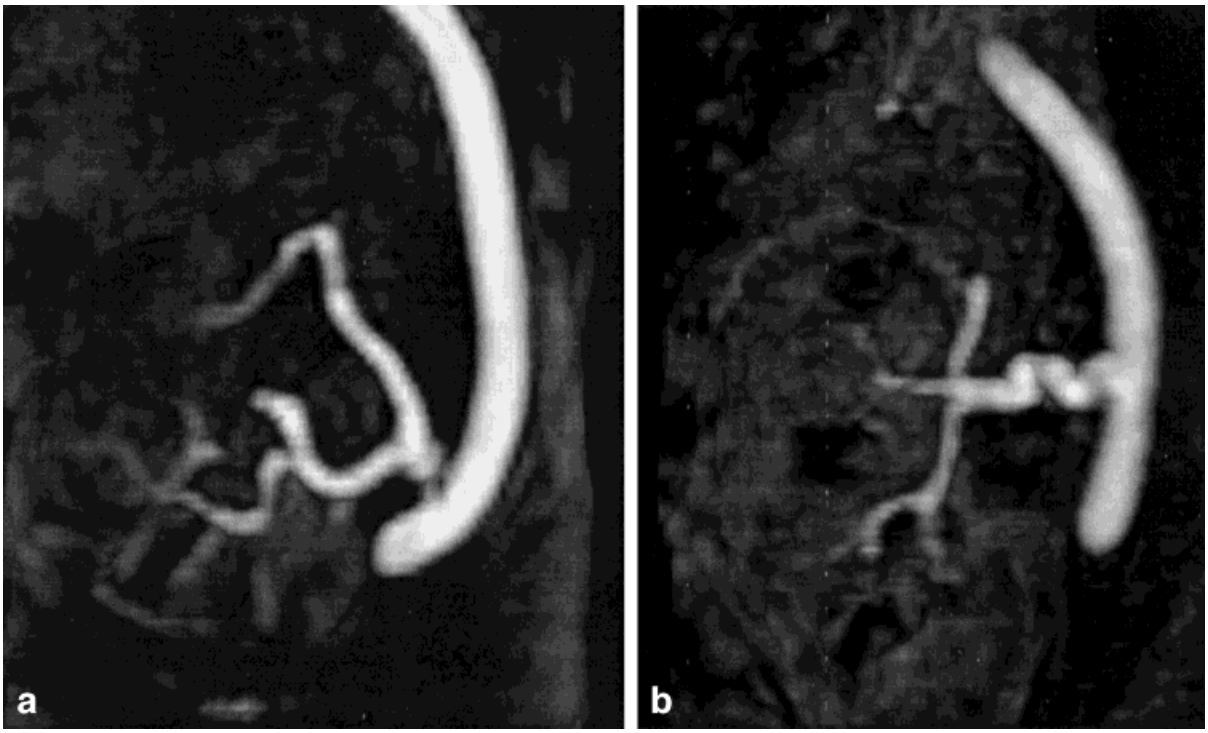

Figure 8. (**a**) Severe stenosis at the anastomosis site well depicted in 3D Gd-MRA (arrow). The site of anastomosis was difficult to assess in DSA due to the orientation and overlapping arteries. (**b**) 3D Gd-MRA MIP reformat showing kinking of the transplant renal artery.

Impairment of arterial flow to the renal transplant may be caused by stenosis of the allograft vessels commonly at the site of anastomosis, kinking (Fig. 8b) or inflow disease proximal to the anastomosis caused by occlusion or significant stenosis of the common iliac, or external iliac artery ipsilateral to the allograft (Fig. 9). Prior transplantation assessment of the pelvic vascular anatomy with 3D-contrast enhanced MRA may be use-

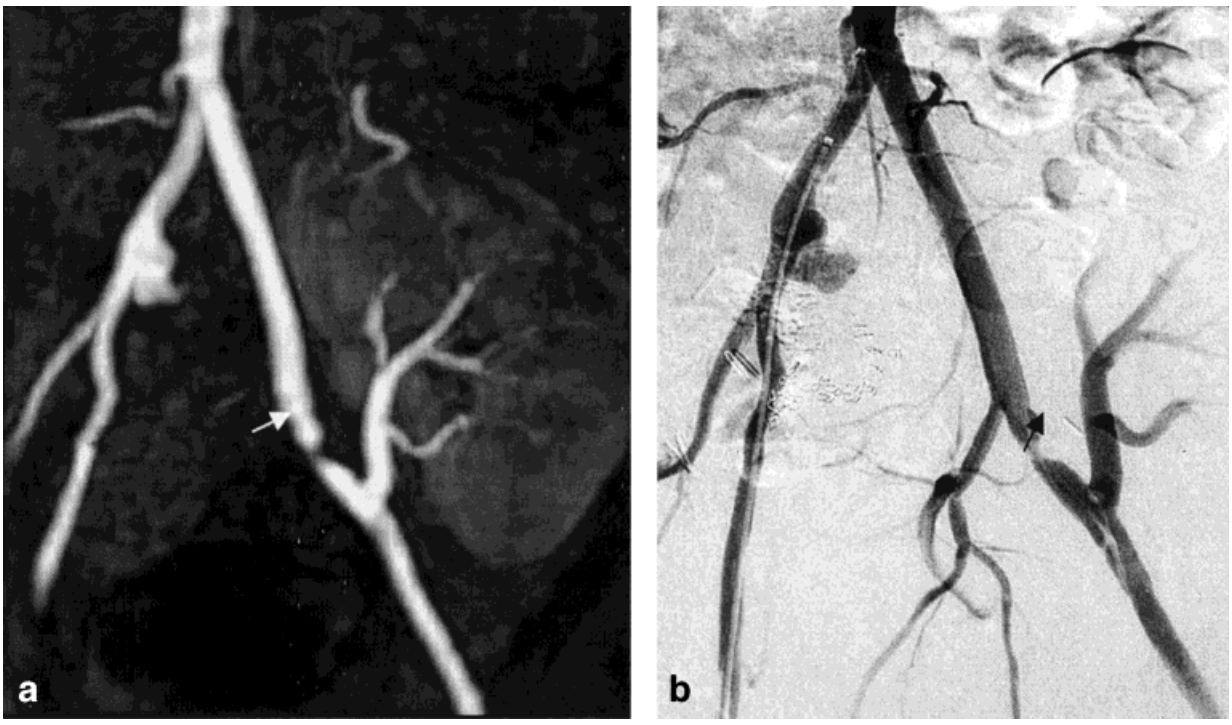

Figure 9. Severe stenosis proximal to the transplant artery anastomosis. Coronal MIP from 3D Gd-MRA (left). DSA (right). The transplant artery and anastomosis are patent.

ful in high-risk group including diabetics and chronically hypertensive patients.

There are a few pitfalls that may lead to the false diagnosis of stenosis or overestimation of a stenosis. Artifacts caused by metallic surgical clips near the transplant artery may result in signal drop overlying the vessel, giving the false impression of stenosis (Fig. 10). Careful evaluation of the spin echo images and the 3D Gd-MRA source images will show this signal drop in both renal artery and vein. Another characteristic finding of the metallic clip artifact is bright signal at the margin of the signal drop in the soft tissue next to the renal allograft. Another pitfall may be caused by venous overlaps due to inaccurate timing of the arterial bolus. Careful evaluation of the source images and multiplanar reformats frequently solve this problem (15).

Renal Artery Thrombosis

Renal artery thrombosis is a rare complication occuring in 1% of cases. Thrombosis of the main renal artery usually results in the loss of the renal allograft if not detected and managed early. It may occur in the first 2 weeks after transplantation. The most common causes of renal allograft artery thrombosis are hyperacute rejection, hypercoagulapathy and high cyclosporine doses. Other less common causes of the allograft renal artery thrombosis are dissection, malanastomosis, kinking, or torsion of the transplant around its vascular pedicle (26). Clinically this presents as decrease or no urine output in a previously functioning renal allograft.

The MR findings of infarcted allograft includes normal or heterogeneous signal on T1 and T2 WI from hemorrhagic necrosis (30). If the transplanted kidney has two renal arteries, segmental infarction may occur if one artery is occluded. Small infarcts may not cause abnormal signal in T2 WI. On post-contrast fat saturated T1 WI the infarcted allograft shows no parenchymal enhancement or slight linear enhancement of the inner renal parenchyma in case of main renal artery occlusion.

Helenon et al. described variable patterns of allograft necrosis on post gadolinium enhanced images: small cortical focal area, large isolated area of infarction, outer cortical necrosis, cortical necrosis with large patches, diffuse cortical necrosis, and both cortical and medullary necrosis (30). Dynamic gadolinium enhanced images are more sensitive than T1 and T2 WI in depicting areas of allograft infarction. It appears as low signal area relative to the high signal enhancing parenchyma. The 3D reformations in multiple planes will confirm the diagnosis by demonstrating non-visualization or absent flow in the transplant renal artery. The thrombus in the renal artery may be seen as low signal filling defect within the renal artery.

Renal Transplant Torsion

Torsion occurs when the renal allograft rotates around its vascular pedicle. It may result in vascular occlusion, depending on the degree of torsion. This rare complication has been described in intaraperitoneal transplant kidneys and may occur early in the postoperative period

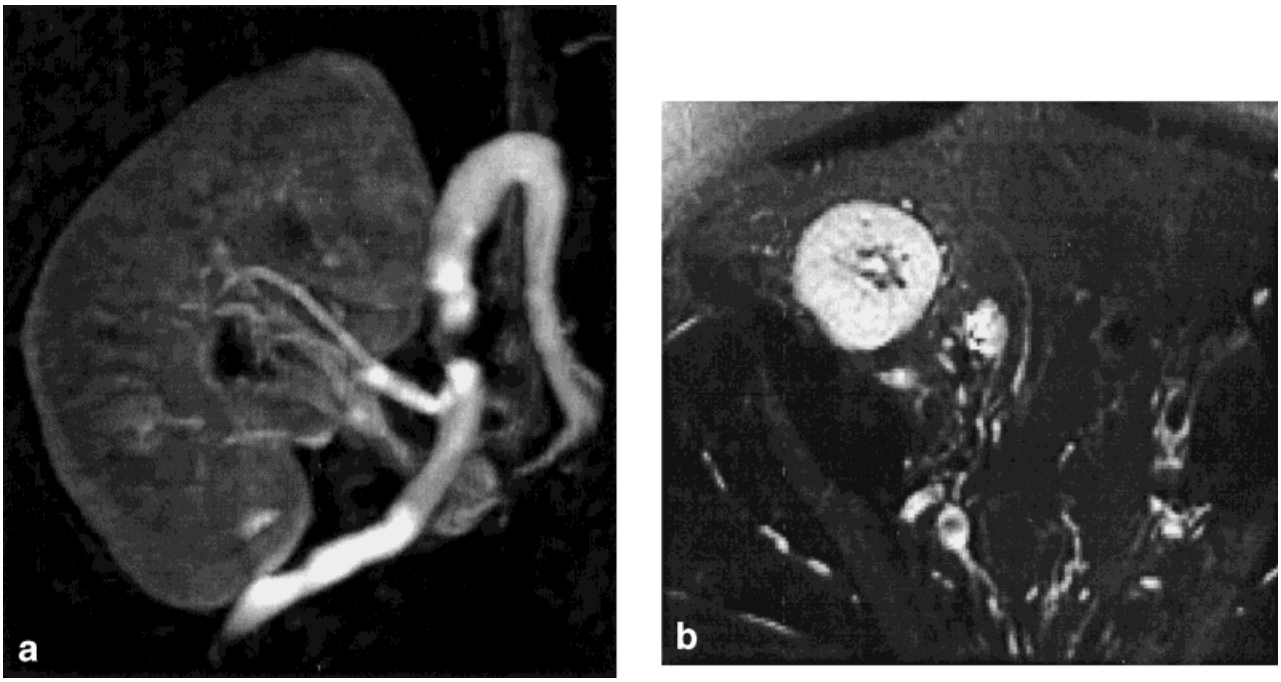

Figure 10. Clip artifact produced false positive stenosis. (**a**) Coronal oblique MIP reformat from 3D Gd-MRA demonstrating signal drop overlying the transplant artery related to metallic clip artifact giving the false impression of external iliac artery stenosis. (**b**) Axial T2 Fast spin echo demonstrating high signal adjacent to the artifactual signal void area produced by the metallic surgical clip near the anastomosis.

or as late as 6 months. MRI may show an enlarged kidney with or without renal hemorrhage. Slow flow in the renal vessels may be depicted as intravascular signal (31).

Renal Vein Thrombosis

Renal vein thrombosis occurs in 0.3 to 4% of cases. Frequently seen in the postoperative period. Since the clinical symptoms are non-specific, therefore the diagnosis is often made after the allograft has infarcted. Thrombosis of the renal vein compromises arterial flow resulting in allograft infarction (31). MRI demonstrates an enlarged renal allograft, diminished or absent CMD, focal areas of parenchymal infarcts. There is no enhancement of the renal allograft on MRA and the thrombosed renal vein is also not visualized. Subtle linear enhancement of the inner parenchyma of the allograft may be seen. Subcapsular hemorrhage may also be observed (Fig. 11).

Lymphocele

The incidence of lymphocele following renal transplantation occurs between 1 to 18% of cases. It is considered the most common cause of peritransplant fluid collection. Lymphoceles that occur in the first month are often related to the surgery. Late occurrence is often related to rejection (26). They are frequently located inferior and medial to the renal allograft. Lymphocele is of low signal on T1 and high signal on T2 WI. Thin internal septa may be present (32). The majority of the lymphoceles are small and asymptomatic. Occasionally they become large enough to cause urinary obstruction

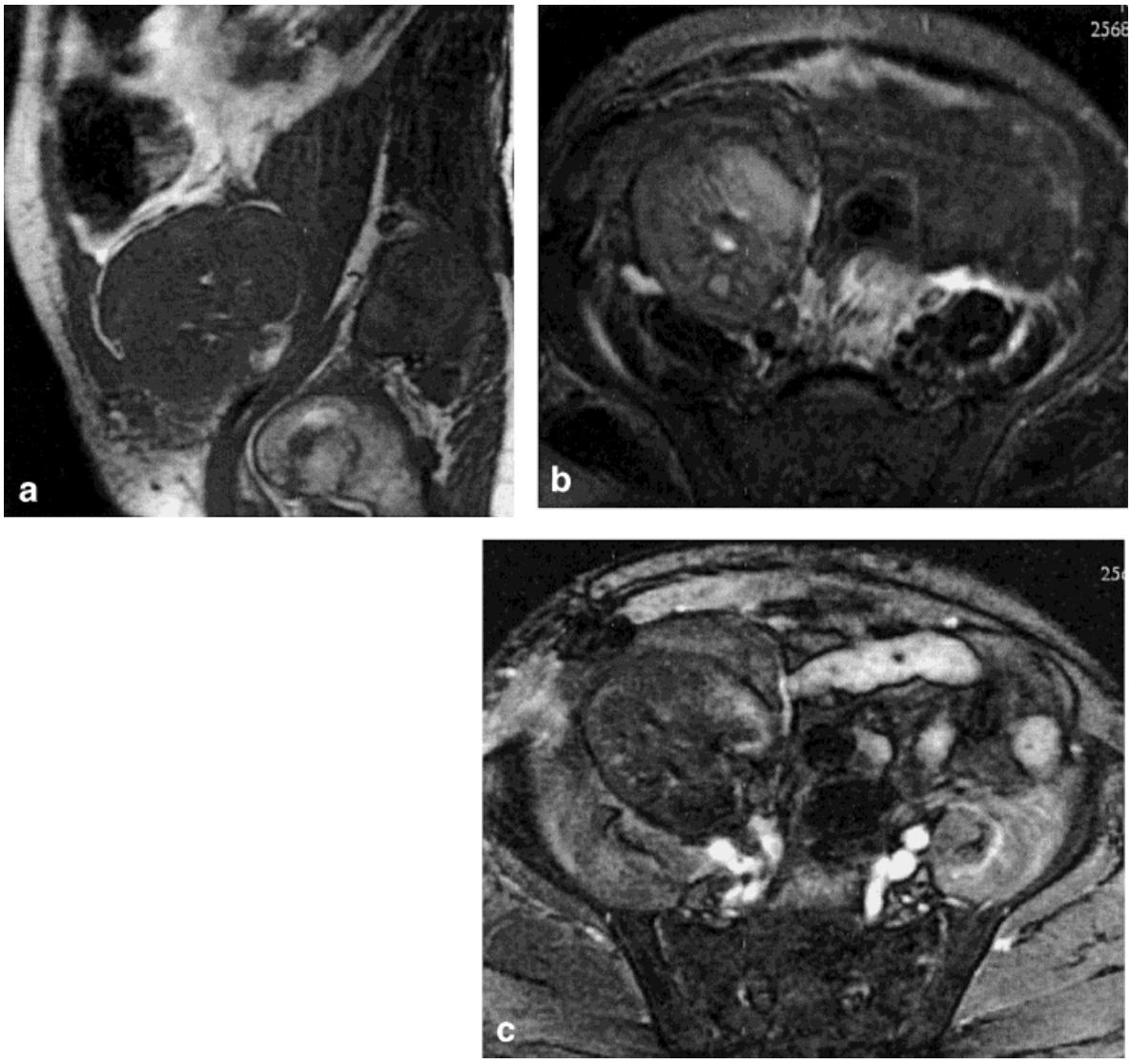

Figure 11. Renal allograft infarction cased by transplant renal vein thrombosis. **a:** Sagital T1 WI spin echo. **b:** Axial T2 WI demonstrating enlarged renal allograft with loss of normal CMD and sinus fat. The subcapsular hematoma has slightly higher signal than renal parenchyma in T1 and T2 (arrowhead). **c:** Axial image obtained after 3D Gd-MRA demonstrating lake of normal enhancement of the renal allograft with only subtle linear enhancement of the inner medulla and small area in the anterior cortex, a pattern described in renal infarction.

by compressing the ureter, the transplant vessels, or the allograft parenchyma (Fig. 4).

Hematoma

Hemorrhage occurring at the site of the anastomosis may require urgent surgical intervention. Nonanastomotic postoperative hemorrhage is not uncommon (26). MRI easily diagnoses this complication. The hemorrhagic fluid collection appears as high signal in both T1 and T2 WI. The heterogeneous signal of the hemorrhagic fluid differentiates it from other causes of peritransplant fluid collections. Hemorrhage may occur in the allograft parenchyma or in the subcapsular or region.

Urinoma

Urinoma is an early complication, occurring early in the first 5 weeks after transplantation due to leakage of urine from the anastomotic site at the hilus of the renal transplant. The incidence of this varies between 3 to 10%. It requires urgent surgical or radiological intervention (32). The signal characteristic of the urinoma is non-specific low on T1 and high on T2 WI. Lymphocele and seroma have similar signal intensities. Percutaneous aspiration of the fluid collection under ultrasound guidance will provide the definitive diagnosis. Scintigraphy may also help in differentiating urinary leakage from lymphocele or seroma by detecting free leakage of the ^{99m}Tc-DTPA into the peritoneum.

Cyclosporine Toxicity

The MR findings of cyclosporine toxicity in the renal allograft are varied. The allograft is often normal in size, signal, and CMD. However, enlargement of the allograft and diminished or even absent CMD have been described.

Rejection

Allograft rejection results in increase in the T1 shortening of the renal cortex compared to the medulla and is related to interstitial edema of the renal cortex. This is depicted as decreased cortical signal on T1 WI best seen in the immediate post gadolinium enhanced fat suppressed images or fat suppressed T1 WI. Many authors consider the loss of CMD as the most consistent MR finding in allograft rejection (33–35). The degree of CMD loss roughly corresponds to the severity of the rejection (36). Hricak et al. described high MRI accuracy in diagnosing rejection compared to scintigraphy and US, 98%, 75%, and 72%, respectively (37). Unfortunately this finding is non-specific for rejection and may be seen in acute tubular necrosis, renal artery thrombosis, cyclosporine toxicity, and infectious nephritis. Because of this overlap, some authors considered CMD as being non-specific to diagnose rejection (38–40). Posttransplant lymphoproliferative disease is another cause of loss of CMD. This can be differentiated from rejection by the minimal or lacks of contrast enhancement in posttransplant lymphoproliferative disease but not with rejection, but failure of the allograft to enhance after gadolinium chelate injection may occur in severe ATN similar to posttransplant lymphoproliferative disease. The sinus fat may become ill defined in rejection. The appearance of the rejected allograft on T2 WI is variable ranging from normal to increased cortical signal relative to the medulla. Heterogeneous signal intensity or even low cortical signal has been described. The kidney may or may not enlarge.

Acute Tubular Necrosis

ATN is most frequently seen in the cadaveric allograft due to the long ischemia time between harvesting and

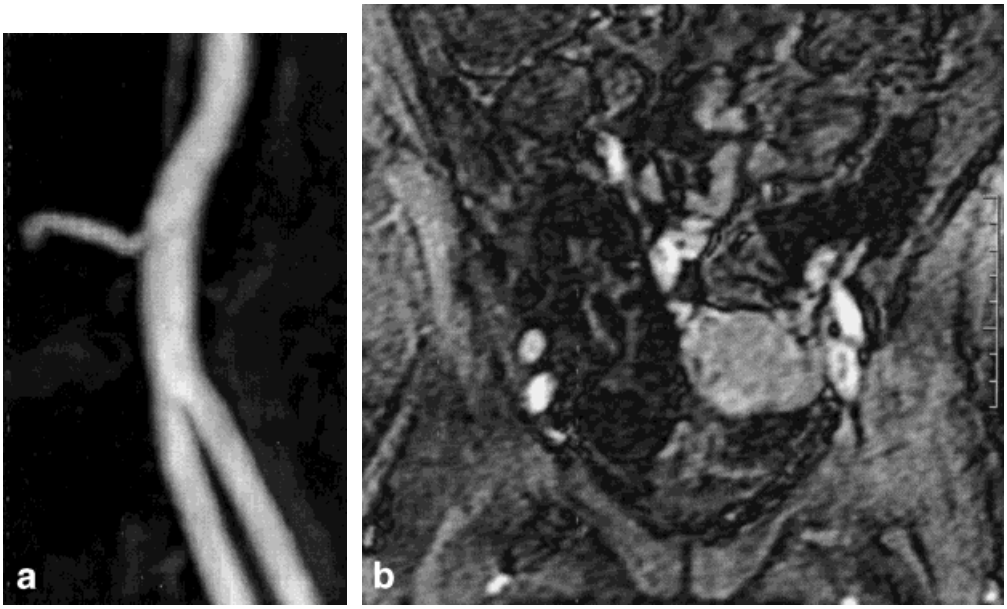

Figure 12. Severe acute tubular necrosis. **a:** 3D Gd-MRA reformat showing patent transplant renal artery. **b:** A source image from the second phase 3D Gd-MRA demonstrating lack of renal allograft enhancement compares to the enhancing uterus.

grafting. This occurs in the first week posttransplantation but can occur later. ATN has variable appearance on MR particularly in the cadaveric allograft. The CMD may be normal, decreased or even absent (Fig. 12). Geisinger et al. suggested that CMD analysis be of a little value in ATN of the cadaveric renal transplant (36). Some authors reported preserved CMD in ATN in living donor-related allograft, compared to the loss of CMD in rejection (34,37). However, owing to the overlap between ATN, cyclosporine toxicity, and rejection, allograft biopsy is frequently needed for definitive diagnosis.

POSTTRANSPLANTATION LYMPHOPROLIFERATIVE TUMORS

Lymphoreticular malignancies and skin malignancies have been reported to be more frequent in immunosuppressed patients than in the general population (42). Malignant lymphoma (commonly non-Hodgkin type) and cyclosporine-induced lymphoproliferative disorder (PTLD) have been described post kidney transplantation. The incidence of PTLD is 2%. It almost always occurs in Epstein-Barr virus positive patients (44). It commonly occurs 2 to 8 months after transplantation, it may regress or completely disappear after reduction of the cyclosporine dose. The sites of involvement are lymph nodes, gastrointestinal tract, lungs, and brain. The allograft may be affected but to a lesser degree than with posttransplantation lymphoma (43,44). Ali et al. described predilection of PTLD to occur as a mass in the renal hilum that encases the hilar vessels of the renal allograft. When renal parenchyma is involved, it tends to be as multiple lesions. PTLD appears as hypointense mass on T1 and T2 WI with minimal enhancement after gadolinium contrast (45). Using MRI as complementary to ultrasound or CT may be useful to diagnose this entity. Other abnormalities that can be difficult to be differentiated from PTLD are lymphoma, rejection, and peritransplant hematoma.

Contrast enhancement may favor peritransplant PTLD over hematoma particularly if there is encasement of the renal hilar vessels.

SUMMARY

MR angiography is a reliable diagnostic modality in the evaluation of renal allograft vascular complications. It may be used as a primary modality if vascular complication is highly suspected or following ultrasound MRI is complementary to ultrasound or computed tomography in the characterization of abnormalities to reach a specific diagnosis.

REFERENCES

1. Trusler LA. Simultaneous kidney-pancreas transplantation. ANNA J 1991;18:487–491.
2. Buzzas GR, ShieldIII CF, Pay NT, Neuman MJ, Smith JL. Use of gadolinium-enhanced, ultrafast, three-dimensional, spoiled gradient-echo magnetic resonance angiography in the preoperative evaluation of living renal allograft donors. Transplantation 1997;64:1734–1737.
3. Low RN, Martinez AG, Steinberg SM, et al. Potential renal transplant donor: Evaluation with gadolinium-enhanced MR angiography and MR urography. Radiology 1998;207:165–172.
4. Gourlay WA, Yucel EK, Hakaim AG, et al. MRA in the evaluation of living-related renal donors. Transplantation 1995;60:1363–1366.
5. Tsude K, Murakami T, Kim T, et al. Helical CT angiography of living renal donors: comparison with 3D Fourier transformation phase-contrast MRA. J Comput Assist Tomogr 1998;22:186–193.
6. Yanagisawa T, Otsubo O, Yajima A, et al. Magnetic resonance angiography in renal allografts comparison with color doppler echography. Transplantation 1996;28:1533–1534.
7. Nelson HA, Gilfeather M, Holman JM, Nelson EW, Yoon HC. Gadolinium-enhanced breath-hold three-dimensional Time-of-Flight renal MRA in the evaluation of potential renal donors. JVIR 1999;10:175–181.
8. Kadir S. Atlas of normal and variant angiographic anatomy. 1991. W.B. Saunders Company.
9. Strauser GD, Stables Dp, Weil R. Optimal technique of renal arteriography in living related transplant donors. AJR 1978;131: 813–816.
10. Adams MK, Goldsze RC, Pulde MF, Sax EJ, Edelman RR. Renal vasculature in potential renal transplant donors: Comparison of MR imaging and digital sustraction angiography. Radiology 1995; 197:46–472.
11. Prince MR, Narasimahar DL, Stanly JC, et al. Breath-hold gadolinium-enhanced MR angiography of the abdominal aorta and its major branches. Radiology 1995;197:785–792.
12. Holland GA, Dougherty L, Carpenter JP, et al. Breath-hold ultrafast three-dimensional gadolinium-enhanced MR angiography of the aorta and the renal and other visceral abdominal arteries. AJR 1996;166:971–981.
13. De Cobelli F, Vanzulli A, Sironi S, et al. Renal artery stenosises evaluation with breath-hold three dimensional dynamic gadolinium-enhanced versus phase-contrast MRA. Radiology 1997;205:689–695.
14. Khauli R. Surgical aspects of renal transplantation: New approaches. Urol Clin North Am 1994;21:321–341.
15. Prince MR, Grist TM, Debatin JF. 3D contrast MR Angiography. New York: Springer; 1998.
16. Debatin JF, Spritzer CE, Grist TM, et al. Imaging of renal arteries: value of MR angiography. AJR 1991;157:981–990.
17. Silverman JM, Friedman ML, Van Allen RJ. Detection of main renal artery stenosis using phase-contrast cine MR angiography. AJR 1996;166:1131–1137.
18. Gedroyc WMW, Negus R, AL-Kutoubi A, Palmer A, Taube D, Hulme B. Magnetic resonance angiography of renal transplants. Lancet 1992;339:789–791.
19. Schoenberg SO, Knopp MV, Bock M, et al. Renal artery stenosis: grading of hemodynamic changes with MR CINE phase-contrast flow measurements. Radiology 1997;203:45–53.
20. Knesplova L, Krestin G. Magnetic resonance in assessment of renal function. Eur Radiol 1998;8:201–211.
21. Huch Boni RA, Debatin JF, Krestin GP. Contrast-Enhanced MR imaging of the kidneys and adrenal glands. MRI Clin North Am 1996;4:101–131.
22. Ros PR, Gauger J, Stoupis C, et al. Diagnosis of renal artery stenosis: feasibility of combining MR angiography, MR renography and gadopentate-based measurements of glomerular filtration rate. AJR 1995;165:1447–1451.
23. Sharma RK, Gupta RK, Poptani H, et al. The magnetic resonance renogram in renal transplant evaluation using dynamic contrast-enhanced MR imaging. Transplantation 1995;59:1405–1409.
24. Rothpearl A, Frager D, Subramanian A, et al. MR urography: technique and application. Radiology 1995;194:125–130.
25. Knopp MV, Doersam J, Oesingmann N, et al. Functional MR urography in patients with kidney transplantation. Radiologe 1997; 37:233–238.
26. Amante JM, Kahan BD. Technical complications of renal transplantation. Surg Clin North Am 1994;74:1117–1131.
27. Debatin Jf, Sostman HD, Kenleson M, Argabright M, Spritzer CE. Renal magnetic resonance angiography in the preoperative detection of supernumerary renal arteries in potential kidney donors. Invest Rad 1993;28:882.
28. Meyers SP, Talagala SL, Totterman S, et al. Evaluation of the renal arteries in kidney donors: value of three-dimensional phase-contrast MR angiography with maximum-intensity-projection or surface rendering. AJR 1995;164:117.

29. Ferreiros J, Mendez R, Jorquera M, et al. Using gadolinium-enhanced 3D MRA to assess arterial inflow stenosis after kidney transplantation. AJR 1999;172:751–757.
30. Helenon O, Attlan E, Legendre C, et al. Gd-DOTA-Enhanced MR imaging and color doppler US of renal allograft necrosis. Radiographics 1992;12:21–33.
31. Wong-You-Cheong JJ, Grumbach K, Krebs T, et al. Torsion of intraperitoneal renal transplants: Imaging appearances. AJR 1998; 171:1355–1359.
32. Letourneau JG, Day DL, Ascher NL, Castaneda-Zuniga WR. Imaging renal transplants. AJR 1987;150:833–838.
33. Hricak H, Terrier F, Demas B. Renal allografts: evaluation by MR imaging. Radiology 1986;159:435–441.
34. Rholl KS, Lee JK.T, Ling D, Sicard GA, Griffith RC, Freeman M. Acute renal rejection versus acute tubular necrosis in a canine model: MR evaluation. Radiology 1986;160:113–117.
35. Leung AW, Bydder GM, Steiner RE, Bryant DJ, Young IR. Magnetic resonance imaging of the kidneys. AJR 1984;143:1215–1227.
36. Geisinger MA, Risius B, Jordan M, Zelch MG, Novick AC, George CR. Magnetic resonance imaging of renal transplants. AJR 1984; 143:1229–1234.
37. Hricak H, Terrier F, Marotti M, et al. Posttransplant renal rejection: comparison of quantitative scintigraphy, US, and MR Imaging. Radiology 1987;162:685–688.
38. Steinberg HV, Nelson RC, Murphy FB, et al. Renal allograft rejection evaluation by doppler US and MR imaging. Radiology 1987;162:337–342.
39. Winsett MZ, Amparo EG, Fawcett HD, et al. Renal transplant dysfunction. AJR 1988;150:319–323.
40. Lund G, Letourneau JG, Day DL, Crass JR. MRI in organ transplantation. Radilo Clic North Am 1987;25:281–287.
41. Hoover R, Fraumeni JF JR. Risk of cancer in renal transplant recipients. Lancet 1973;2:55–57.
42. Nalesnik MA, Makowaka L, Starzl TE. The diagnosis and treatment of posttransplant intrahepatic Lymphoproliferative disorders. Curr Probl Surg 1988;25:365–472.
43. Harris KM, Schwartz ML, Slasky BS, Nalesnik MA, Makowaka L. Posttransplantation Cyclosporine-induced Lymphoproliferative disorders: clinical and radiologic manifestations. Radiology 1987;162: 697–700.
44. Strouse PJ, Platt JF, Francis IR, Bree R. Tumorous intrahepatic Lymphoproliferative disorder in transplanted livers. AJR 1996;167: 1159–1162.
45. Ali MG, Coakley F, Hricak H, Bretan PN. Complex posttransplantation abnormalities of renal allograft: evaluation with MR imaging. Radiology 1999;211:95–100.